

General Projective Maps for Multidimensional Data Projection

Dirk J. Lehmann and Holger Theisel¹

¹Department of Simulation and Graphics, University of Magdeburg, Germany

Abstract

To project high-dimensional data to a 2D domain, there are two well-established classes of approaches: RadViz and Star Coordinates. Both are well-explored in terms of accuracy, completeness, distortions, and interaction issues. We present a generalization of both RadViz and Star Coordinates such that it unifies both approaches. We do so by considering the space of all projective projections. This gives additional degrees of freedom, which we use for three things: Firstly, we define a smooth transition between RadViz and Star Coordinates allowing the user to exploit the advantages of both approaches. Secondly, we define a data-dependent magic lens to explore the data. Thirdly, we optimize the new degrees of freedom to minimize distortion. We apply our approach to a number of high-dimensional benchmark datasets.

Categories and Subject Descriptors (according to ACM CCS): I.3.3 [Computer Graphics]: Picture/Image Generation—Information Visualization

1. Introduction

Finding suitable projections from points in a high-dimensional data space to the 2D visualization space is one of the standard problems in Information Visualization, and it is still a hard one. The reason for this is two-fold: Firstly, every projection comes with distortions, an effect that should be minimized as much as possible. Secondly, the space of all possible projections is infinite.

There are two classes of standard projection techniques: non-linear projections, such as RadViz [HGM*97], and linear projections, such as Star Coordinates [Kan00]. Both are well-explored in terms of distortion minimization, cluster discrimination, and placement (both interactive and automatic) of the coordinate points/axes, respectively. However, both projection techniques have been explored rather independent of each other.

In this paper, we present an approach to unify both techniques. We achieve this by considering the space of all projective projections from the data space to the visualization space. A projective projection preserves the cross ratio of four collinear points and is considered as umbrella term that joins non-linear, linear, and affine projections. Since RadViz treats a certain subset of projective maps and Star Coordinates feature the space of all affine projections, both RadViz and Star Coordinates appear as special cases in our new approach. The new approach has more degrees of freedom than RadViz or Star Coordinates. Our approach to visualize and interact with them is to have for every dimension a 2D coordinate axis together with a weight point moving on this axis. Both the axes and the weight points can be interactively moved or automatically set by certain optimization approaches.

Having more degrees of freedom for finding suitable projections

is not per se an advantage, especially when good projections are searched in a purely interactive process. Therefore, we need approaches to automatically adjust or optimize the new degrees of freedom to get better projections than RadViz or Star Coordinates alone. To address this, we propose three approaches:

- We propose a scheme of interpolation between RadViz and Star Coordinates, allowing to exploit the advantages of both techniques.
- We use the new degrees of freedom to introduce a data-dependent magic lens function working in the visualization space. It allows to get more information about the relations in data space from their projections.
- We use the new degrees of freedom to establish an axis-based interaction scheme that minimizes projection-related distortions during the exploration of the space of projective projections.

2. Related Work

The visualization of nD data is still challenging and thus various techniques exist [CCKT83, Fri91]. Especially the use of projection techniques has been established in recent years. They define a mapping of n -dimensional data to a 2D visualization space, to reduce dimensionality and to get insights into data patterns. Integrated tools exist providing the use of different projection approaches, such as DimStiller [IMI*10]. Such projection techniques are systematized in *projective projections*, *affine projections*, *distance-based projections*, and their interactive applications.

Projective projections map straight lines to straight lines and preserve the cross ratio of four collinear points [Far02, LT13]. A family of multivariate projective embeddings has been introduced by Hoffman et al. as Radial Visualizations (RadViz) [HGM*97, HGP99,

Nv06, DCFMFM10, DGRG12]. It introduces non-linearity in the projection process by using an additional weighting factor based on an underlying spring model. Theisel and Kreuseler [TK98] presented a related variation to reveal a representative closed free-form surface from the data. Additionally, normalized RadViz is given by Daniels et al. [DGRG12], which investigates ordering properties. Nováková et al. [Nv11, Nv06, Nov09] and DiCaro et al. [DCFMFM10] described characteristic properties of RadViz. They also stressed that misleading distortions might be introduced due to the non-linearity of RadViz.

Affine projections map straight lines to straight lines and preserve the ratio of three collinear points [Far02, LT13]. Kandogan et al. [Kan00, Kan01] introduced multivariate affine Star Coordinates. They define a linear multivariate projection from nD data to a 2D visualization domain enabling a multivariate visual data analysis. Star Coordinates also introduce additional distortions, which leads to confusion during a visual search. In order to reduce such distortion effects, the multivariate Orthographic Star Coordinates (OSC) [LT13] establish a set of constraints that facilitate to preserve an orthographic multivariate projection. Some popular projection techniques are naturally orthographic, such as principal component analysis (PCA) or traditional bivariate scatterplots, which are both a subset of the OSC. A comparison between affine Star Coordinates and projective RadViz has been given in [RS-DRS15]. Additionally, perception properties of such projections were considered, e.g., in [EMdSP*15]. In this work, we unify both affine and projective projections and we present a generic concept for multivariate projections.

Distance-based projections optimize a certain distance measure to reveal a projection of interest. In fact, they can be both an affine or a projective projection and thus they are “orthogonal” to the former mentioned techniques. The Multidimensional scaling (MDS) [Tor52] preserves distances between the data records under projection and they are based on the eigenvalues of the data-related distance matrix. With Glimmer [IMO09], a high-performance approach for multilevel MDS on graphic processing units is known and Cheng and Mueller [CM16] propose to combine both the similarity of dimensions and of data records to one concept of a *fully* MDS. Paulovich et. al [PSN10] introduce the part-linear multidimensional projection (PLMP) to speed up the projection process by reducing the number of required distance samples from the data. Additionally, a local affine multivariate projection (LAMP) [JCC*11] is known: for this, interactively placed 2D seed points control and steer the distance-minimizing process regarding the projected data and the seed points themselves. The inverse affine multidimensional projection (iLAMP) [ABD*12] goes the inverse direction and it projects image points from the 2D visualization space back to the space of high-dimensional data by minimizing nearest neighbor distances of the image points and the data records in a least-square sense. Another error minimization approach, which has been applied to a set of different projection techniques, was presented in [CM15] by focusing on radial layout configurations. Our approach neither focus on a certain layout scheme nor on different projection techniques. Instead, we consider the complete space of projections in one technique. Additionally, we present a novel distortion minimization concept (and a concept of a magic lens) for our General Projective Maps that are also based on a minimization of distances in the projection space.

Interactive Projection Applications are given by either interactively manipulate the projection matrix – based on user input w.r.t control points (cf. anchor points), data input, or parameters – or by running an optimization in the background to provide a set of optimal projections as a sort of a data tour.

Regarding this, a set of interaction techniques, e.g., for PCA-based projections is provided [JZF*09], such as a jitter operation to reduce clutter or by steering certain weights to control the influence of variables to the projection. To go the other way around is proposed in [NM13] by using a direct data manipulation and interaction concept in order to investigate their influence under a certain projection model and parameterization as well. To interact with the projection space itself is proposed in [EHM*11] w.r.t. a tourism business case.

Data tours are a set of traditional approaches in order to successively walk through the projection space. Based on low-dimensional projections, Friedman et al. [FT74, Fri87] proposed strategies to get 2D embeddings with patterns of interest for nD data. From this, a time sequence of a set of projections is provided for conducting a visual data exploration. The projection pursuit [FT74, CBCH95] and the grand tour [Asi85] provide a greedy tour of (bivariate) projections, which exponentially grows with the number n of data dimensions. They allow to intuitively detect patterns of interest in the data, but they are time-consuming, especially with growing n . Later, short and complete data tours with a number of $n/2$ different multivariate projections have been introduced [LT15]. Nowadays, it has become customary to explore interactively the space of low-dimensional projections by controlling a related parameter set, such as the projection’s anchor points (cf. [SDMT15]). Thus, a data tour has become an interaction concept instead of just being presented as a sequence after a fully automatic preprocessing. We present a data tour-like interactive exploration scheme that automatically selects optimal projective coefficients in order to handle the degree of freedom of our General Projective Maps, and in order to discard distortion during the exploration of the space of projective projections. In the following, we present our concept of General Projective Maps.

3. Theory of General Projective Maps

We denote \circ as the Schur (Hadamard) product of two matrices of equal size, “diag” denotes the diagonalization matrix of a vector. $\mathbf{0}_{i,j}$ and $\mathbf{1}_{i,j}$ are $i \times j$ matrices with all entries 0 and 1, respectively. We omit the indices if the dimensionality is clear from the context.

Let n be the dimensionality of the data space, and let m be the number of present data points. Then the j -th point in the data space can be written as $\mathbf{d}_j = (d_{1,j}, \dots, d_{n,j})^T$, and the matrix of all data points is the $n \times m$ data matrix

$$\mathbf{D} = (\mathbf{d}_1, \dots, \mathbf{d}_m). \quad (1)$$

Star Coordinates define a 2D coordinate axis \mathbf{a}_i for every dimension, while RadViz defines an anchor point that can be interpreted as a position vector. This way, for both Star Coordinates and RadViz, the projection is defined by a $2 \times n$ projection matrix

$$\mathbf{A} = (\mathbf{a}_1, \dots, \mathbf{a}_n). \quad (2)$$

In Star Coordinates, the 2D projection \mathbf{x}_j of an nD point \mathbf{d}_j is

$$\mathbf{x}_j = \mathbf{A} \cdot \mathbf{d}_j \quad (3)$$

while in RadViz we have

$$\mathbf{x}_j = \frac{\mathbf{A} \cdot \mathbf{d}_j}{\sum_{i=1}^n d_{i,j}}. \quad (4)$$

For Star Coordinates the matrix \mathbf{X} of all projected data points is

$$\mathbf{X} = \mathbf{A} \cdot \mathbf{D} \quad (5)$$

and for RadViz

$$\mathbf{X} = \mathbf{A} \cdot \mathbf{D} \cdot \text{diag} \left(\frac{1}{\sum_{i=1}^n d_{i,1}}, \dots, \frac{1}{\sum_{i=1}^n d_{i,m}} \right). \quad (6)$$

Our approach is based on a representation of both the data and the projection matrix in *homogeneous coordinates*. For this, we define the *homogeneous data matrix* as

$$\bar{\mathbf{D}} = \begin{pmatrix} \mathbf{D} \\ 1, \dots, 1 \end{pmatrix} \quad (7)$$

and the *homogeneous projection matrix* as the $3 \times (n+1)$ matrix

$$\bar{\mathbf{A}} = \begin{pmatrix} \mathbf{A} & \mathbf{0}_{2,1} \\ \mathbf{c} & 1 - \frac{\mathbf{c} \cdot \mathbf{1}_{n,1}}{n} \end{pmatrix} \quad (8)$$

with $\mathbf{c} = (c_1, \dots, c_n)$. Fig. 1c illustrates $\bar{\mathbf{A}}$. Then, we get for the projected points in homogeneous coordinates

$$\bar{\mathbf{X}} = \bar{\mathbf{A}} \cdot \bar{\mathbf{D}} = \begin{pmatrix} \mathbf{x}_1, \dots, \mathbf{x}_m \\ w_1, \dots, w_m \end{pmatrix} = \begin{pmatrix} \mathbf{A} \cdot \mathbf{D} \\ \mathbf{w} \end{pmatrix} \quad \text{with} \quad (9)$$

$$\mathbf{w} = (w_1, \dots, w_m) = \mathbf{1}_{1,m} + \mathbf{c} \cdot \left(\mathbf{D} - \frac{1}{n} \mathbf{1}_{n,m} \right). \quad (10)$$

In the final step, the projected points in Cartesian coordinates are obtained from the projective ones by normalizing them by w_j :

$$\mathbf{X} = \begin{pmatrix} \frac{\mathbf{x}_1}{w_1}, \dots, \frac{\mathbf{x}_m}{w_m} \end{pmatrix}. \quad (11)$$

Note that \mathbf{c} contains the new degrees of freedom that appear in our approach. Also note that RadViz and Star Coordinates are now simple special cases: $\mathbf{c} = (0, \dots, 0)$ gives Star Coordinates while $\mathbf{c} = (1, \dots, 1)$ gives RadViz. Figures 1(a) and 1(b) illustrate the projective projection matrices for RadViz and Star Coordinates.

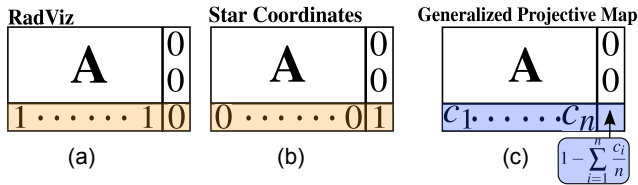


Figure 1: Homogeneous projection matrices.

For the visual representation of the projection matrix $\bar{\mathbf{A}}$, we use standard coordinate axes \mathbf{a}_i on each dimension. On each axis we place a weight point (denoted by a little triangle in the visualization) that can be freely moved on the axis. This is similar to Farin points for rational Bezier curves [Far02]. The weight point in the origin means $c_i = 0$, while the weight point on \mathbf{a}_i means $c_i = 1$. Fig. 2 gives an illustration. Fig. 2b shows that representatives of the projected data are visualized by colored circles. Note that the color encodes the Euclidean distance for each data point in high-dimensional space to its origin, which allows to distinguish data records in the projection space. We draw a solid line from \mathbf{a}_i to the

weight points, while we draw a broken line from the weight points to the origin. This is justified by the following fact: if all c_i are 1 (i.e., if we have RadViz), the origin has no influence on the projection any more; in this case the coordinate axes are anchor points.

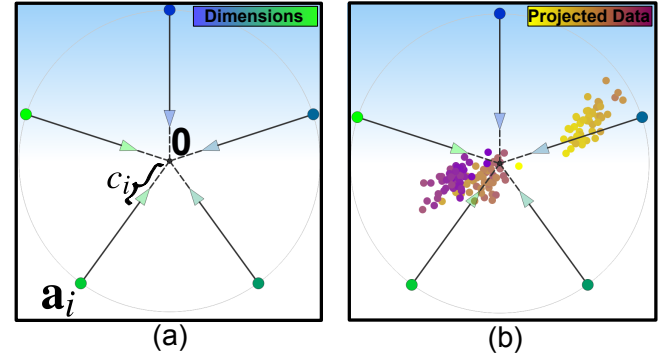


Figure 2: Visualization of the projection parameters \mathbf{a}_i, c_i without projected data (a) and with colored projected data (b).

Given the concept of General Projective Maps, a linear interpolation between RadViz and Star Coordinates can be defined by

$$\mathbf{c} = (t, \dots, t), \quad (12)$$

giving a one-parametric family of projections depending on t . The parameter t is interactively moved by the user; $t = 0$ gives Star Coordinates while $t = 1$ gives RadViz. Note that we do not contribute to the layout of the coordinate axes \mathbf{a}_i here and refer to standard techniques for RadViz or Star Coordinates. Also note that for certain data points \mathbf{d}_j and certain t one can get $w_j = 0$, meaning that the projected point \mathbf{x}_j diverges to infinity. This is a property inherited from RadViz where this could also happen. However, if all data values $d_{i,j}$ are positive and $0 \leq t \leq 1$, we always get $w_j > 0$. Fig. 3 shows a smooth transition between Star Coordinates and RadViz.

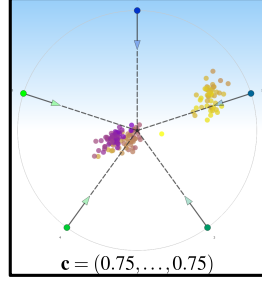
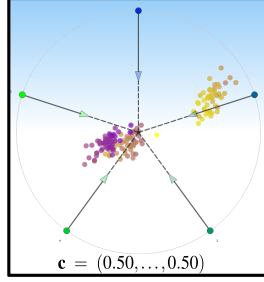
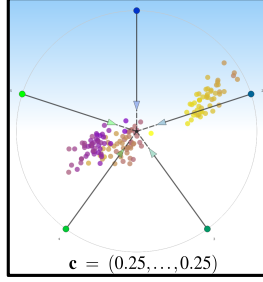
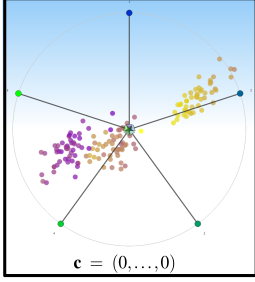
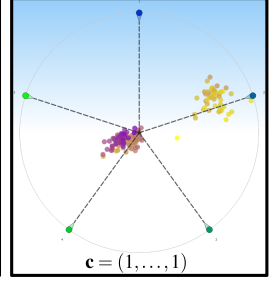
4. Minimizing the Distortion in General Projective Maps

Our General Projective Maps facilitates two interactive and novel approaches to efficiently minimize distortions in the projection space. This goal will be reached by finding a good selection for the projective coefficients \mathbf{c} automatically. Regarding this, we subsequently provide a concept of magic lens, in order to minimize distortions for a subset of the data, and a technique for a global distortion minimization.

4.1. Magic Lens

Magic lenses describe a class of techniques where – within a (usually circular) region – additional information or certain distortions are introduced in the visualization to get more insight [TGK*14, FB95, Fur86, AT82]. Here, we want to modify \mathbf{c} such that we have a magnifying effect, within a certain region, whereas outside the region the visualization is unchanged. The distortion should go beyond a simple distortion in 2D in order to get more information on the spatial relation in the data space.

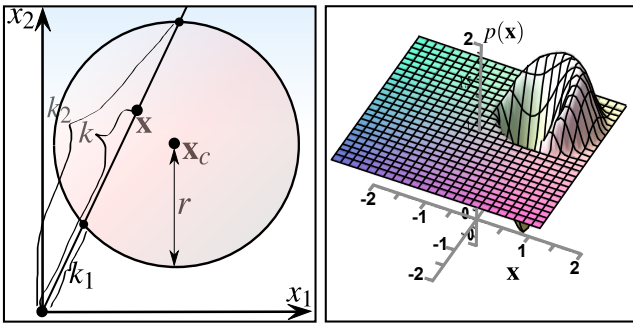
The problem is stated as follows: given the data matrix \mathbf{D} and the projection matrix $\bar{\mathbf{A}}$ consisting of \mathbf{A} and \mathbf{c} , we want to change \mathbf{c} to $\hat{\mathbf{c}}$ such that we obtain a magic lens effect. The magic lens is set by a center \mathbf{x}_c , a radius $r > 0$, and a strength $s > 0$. Before

Star Coordinates

RadViz

Figure 3: Smooth transition between Star Coordinates and RadViz.

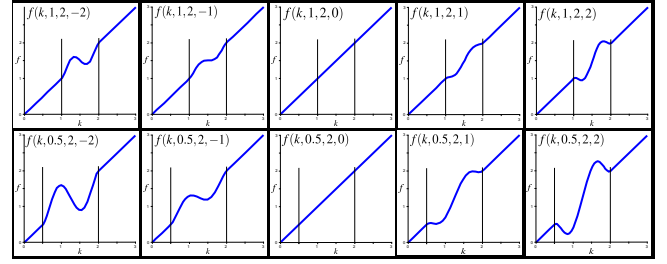
constructing $\hat{\mathbf{c}}$, we realize that changing \mathbf{c} to $\hat{\mathbf{c}}$ results in moving a point \mathbf{x} along the axis through \mathbf{x} and the origin, i.e., it results in a scaling of \mathbf{x} . Here, \mathbf{x} denotes the projected point in the projection space, which is related to the data coordinate \mathbf{d} by $\bar{\mathbf{x}} = \bar{\mathbf{A}} \cdot \bar{\mathbf{d}}$, with $\bar{\mathbf{x}} = (\mathbf{x} \ w)^T$ and $\bar{\mathbf{d}} = (\mathbf{d} \ 1)^T$ (cf. Eq. (9)). Now, we construct $\hat{\mathbf{c}}$ in two steps. Firstly, we define a function $p(\mathbf{x})$ providing a desired scaling of a projected point at \mathbf{x} : if a point is projected by $\bar{\mathbf{A}}$ to $\frac{\mathbf{x}}{w}$, then the change of \mathbf{c} to $\hat{\mathbf{c}}$ should move the projected point to $p\left(\frac{\mathbf{x}}{w}\right) \cdot \left(\frac{\mathbf{x}}{w}\right)$. We construct p in the following way: if \mathbf{x} is outside the circle with radius r around \mathbf{x}_c , we set $p(\mathbf{x}) = 1$. Otherwise, we compute the Euclidean distance k of \mathbf{x} to the origin, i.e., $k = k(\mathbf{x}) = \|\mathbf{x}\|$, as well as the distances k_1, k_2 of the intersection points of the line through \mathbf{x} and the origin with the circle with radius r around \mathbf{x}_c . Fig. 4(left) illustrates the computation of k, k_1, k_2 . Note that this way k, k_2 are non-negative while k_1 can have any sign. Then, we construct a piecewise polynomial function $f(k)$ such that $f(k)$ is a degree 5 polynomial with

$$f(k_1) = k_1, f(k_2) = k_2, \dot{f}(k_1) = \dot{f}(k_2) = 1, \\ f\left(\frac{k_1 + k_2}{2}\right) = \left(\frac{k_1 + k_2}{2}\right), \dot{f}\left(\frac{k_1 + k_2}{2}\right) = 1 + s(k_2 - k_1), \quad (13)$$

for $k_1 \leq k \leq k_2$ and $f(k) = k$ else. In Eq. (13), \dot{f} denotes the first order derivative of f . Note that Eq. (13) uniquely defines a degree 5 polynomial as long as $k_1 < k_2$. We provide a closed solution in monomial form in an accompanying Maple sheet. Fig. 5 illustrates f . Then, we set $p(\mathbf{x}) = f(k(\mathbf{x}))/k(\mathbf{x})$. Fig. 4(right) illustrates $p(\mathbf{x})$.


Figure 4: Computation of $p(\mathbf{x})$ for magic lens effect regarding a projected data point \mathbf{x} and the magic lens parameters \mathbf{x}_c and r , (left) computation of k, k_1, k_2 , (right) resulting $p(\mathbf{x})$ as height field.

In the second step, we complete the new $\hat{\mathbf{c}}$ by an energy minimiza-


Figure 5: Examples of $f(k, k_1, k_2, s), k = 1, \dots, 3$ for several k_1, s .

tion. In fact, we want to find $\hat{\mathbf{c}}$ such that the projected data point $\frac{\mathbf{x}_j}{w_j}$ is moved to $\frac{\mathbf{x}_j}{\hat{w}_j}$ that should be as close as possible to $p\left(\frac{\mathbf{x}_j}{w_j}\right) \cdot \frac{\mathbf{x}_j}{w_j}$

$$\text{where } \hat{\mathbf{w}} = (\hat{w}_1, \dots, \hat{w}_m) = \mathbf{1}_{1,m} + \hat{\mathbf{c}} \cdot \left(\mathbf{D} - \frac{1}{n} \mathbf{1}_{n,m}\right). \quad (14)$$

This is a linear minimization problem. We search for a $\hat{\mathbf{c}}$ that minimizes the quadratic error function

$$\sum_{j=1}^m \left(\hat{w}_j - \frac{w_j}{p\left(\frac{\mathbf{x}_j}{w_j}\right)} \right)^2.$$

Introducing the line vector

$$\mathbf{q} = \left(\frac{w_1}{p\left(\frac{\mathbf{x}_1}{w_1}\right)}, \dots, \frac{w_m}{p\left(\frac{\mathbf{x}_m}{w_m}\right)} \right), \quad (15)$$

it is the solution of the linear system

$$\mathbf{M}_1 \cdot \hat{\mathbf{c}}^T = \mathbf{y}_1 \quad (16)$$

with

$$\mathbf{M}_1 = \left(\mathbf{D} - \frac{1}{n} \mathbf{1}_{n,m}\right) \cdot \left(\mathbf{D} - \frac{1}{n} \mathbf{1}_{n,m}\right)^T \\ \mathbf{y}_1 = \left(\mathbf{D} - \frac{1}{n} \mathbf{1}_{n,m}\right) \cdot (\mathbf{q} - \mathbf{1}_{1,m})^T. \quad (17)$$

Note that the $n \times n$ matrix \mathbf{M}_1 depends on \mathbf{D} only and can therefore (along with its inverse) be pre-computed. This means that changing the location of the magic lens affects only \mathbf{y}_1 and not \mathbf{M}_1 .

4.2. Distortion Minimization

In this section we propose to use the new degrees of freedom to minimize distortion while leaving \mathbf{A} untouched. Given the data

matrix \mathbf{D} and the projection matrix \mathbf{A} , we search for $\hat{\mathbf{c}}$ such that distortion in the projection is minimized. For this, we consider two matrices: $\mathbf{E} = (e_{i,j})$ is a symmetric $m \times m$ matrix such that $e_{i,j} = \|\mathbf{d}_i - \mathbf{d}_j\|$ depicts the Euclidean distance between the i -th and j -th point in data space. $\mathbf{G} = (g_{i,j})$ is a symmetric $m \times m$ matrix such that $g_{i,j} = \|\mathbf{x}_i - \mathbf{x}_j\|$ depicts the Euclidean distance between the projections by \mathbf{A} of the i -th and j -th point in Star Coordinates, i.e., for $\mathbf{w} = (1, \dots, 1)$. We want to find an optimal $\hat{\mathbf{c}}$ such that distances between $(e_{i,j})$ and $(\hat{g}_{i,j}) = \left(\left\|\frac{\mathbf{x}_i}{\hat{w}_i} - \frac{\mathbf{x}_j}{\hat{w}_j}\right\|\right)$ are minimized. This is a non-linear optimization problem. Since we want to interactively move \mathbf{A} , we need an efficient solution. For this, we linearize the problem. In fact, we break it down to the successive solution of two linear problems in the following way: first, we compute the vector $\mathbf{p} = (p_1, \dots, p_m)$ giving the optimal scaling of each projected point to minimize distortion. In a second step, we compute the optimal $\hat{\mathbf{c}}$ to come as close as possible to \mathbf{p} . For the first step we minimize the following error function:

$$\alpha \sum_{i=1}^m \sum_{j=1}^m \left(\frac{p_i + p_j}{2} g_{i,j} - e_{i,j} \right)^2 + \beta \sum_{i=1}^m \sum_{j=1}^m ((p_i - p_j) g_{i,j})^2. \quad (18)$$

The first term in Eq. (18) has the following meaning: assuming p_i and p_j equal, the distance $g_{i,j}$ of \mathbf{x}_i and \mathbf{x}_j is scaled by $\frac{p_i + p_j}{2}$ which should come as close as possible to $e_{i,j}$. The second term enforces that p_i and p_j are approximately equal. The ratio $\frac{\alpha}{\beta}$ influences the result. Throughout this paper we have chosen $\alpha = 0.5$ and $\beta = 0.1$ (see Sec. 5.3.1 for details). Eq. (18) is a quadratic error function in \mathbf{p} . We get its minimizers by the solution of the linear system

$$\mathbf{M}_2 \cdot \mathbf{p}^T = \mathbf{y}_2 \quad (19)$$

with

$$\begin{aligned} \mathbf{M}_2 &= (\alpha + 4\beta) \text{diag}((\mathbf{G} \circ \mathbf{G}) \cdot \mathbf{1}_{m,1}) + (\alpha - 4\beta) (\mathbf{G} \circ \mathbf{G}) \\ \mathbf{y}_2 &= 2\alpha (\mathbf{E} \circ \mathbf{G}) \cdot \mathbf{1}_{m,1}. \end{aligned} \quad (21)$$

The second step, the computation of the optimal $\hat{\mathbf{c}}$, is similar to the magic lens approach in section 4.1: we solve Eq. (16) and Eq. (17) with the only difference that \mathbf{q} in Eq. (17) is

$$\mathbf{q} = \left(\frac{1}{p_1}, \dots, \frac{1}{p_m} \right) \quad (22)$$

where $(p_1, \dots, p_m) = \mathbf{p}$ were computed in the first step.

5. Evaluation

In this section, we conduct and describe a detailed evaluation of our General Projective Maps, the projective magic lens, and the distance minimization for projective coefficients. For evaluation purposes, we present in Sec. 5.1 background information to the evaluation setup. The evaluation of the magic lens concept is treated in Sec. 5.2. In Sec. 5.3, we investigate relevant properties regarding our concept of distance minimization with both a quantitative evaluation in Sec. 5.3.1 and a qualitative evaluation in Sec. 5.3.2.

5.1. Used Benchmark Datasets and Hardware Configuration

From the UCI data base [AN], three high-dimensional benchmark datasets are used: *Iris* [Fis36], *Yeast* [NK91], and *Wdbc* [SWM93]. In detail, the Fisher's *Iris* plants data base consists of 5 dimensions with 150 records. It gives measurements of the sepal as well as the

petal length and width for three iris species. An amount of protein localization sites is given in the *Yeast* dataset, with 10 dimensions and 1484 records. It is usually used to develop probabilistic classification systems in order to predict properties of proteins. The *Wisconsin Diagnostic Breast Cancer* aka *Wdbc* consists of 569 records with 32 metric dimensions each. It contains a set of attributes of cell nucleus measurements that are revealed from breast cancer patients. Note that a potential a priori classification within the data is not within the focus of our approach or even required; thus, such cases are treated as usual dimensions. Furthermore, to guarantee a fair comparison between outcomes, to avoid numerical influence, and to reduce scaling effects, we linearly normalized the data within the interval $[0, 1]$.

Since the introduced concepts shall be tested for interactive use, our experiments run on a small-dimensional mobile workstation with 2.4 GHz 64 Bit Intel chip, with 12 GB RAM and 8 cores in single core and single thread mode on WIN 7 OS. The prototype was done in C++ by using the libraries *QT* 5.1 for GUI support and *Eigen* in order to support numerical matrix calculus. In the following, we discuss results regarding our projective magic lens concept.

5.2. Evaluation of Magic Lens

The visual exploration of projection configurations of interest by utilizing *focus & context* techniques like visual magic lenses is established and accepted by users. Traditional lens concepts usually operate in the visualization space (cf. [LA94]). In contrast, incorporating the data as an additional source of information is a benefit of our projective magic lens. From the performance point of view, this is feasible since our system is based on the data-related matrix \mathbf{M}_1 (cf. Eq. (17)), which can be solved on the fly because it grows in the number of dimensions n , but not in the number of data points m . Note that in practice usually $m \gg n$ applies. By using our lens approach, projected points in the image space that are related to data points, which have different Euclidean distance values to the origin, are shifted in different directions. Clearly, a group of data representatives \mathbf{D}_i that are placed closer to, e.g., the data's origin than another group \mathbf{D}_j , is moved in one direction and the other group in another direction in visualization space. This effect of *spatial separation* is schematically illustrated in Fig. 6(d). Thus, a local stereo vision-like effect [TC90] appears, by alternately enabling and disabling projective magic lenses (compare Fig. 6(b) with Fig. 6(d)), giving an intuitive view on the distance relations of the projected data points of interest w.r.t. the projection configuration of interest. The spatial separation performed by our projective magic lens enables to address three visualization and exploration issues: (a) the *overplotting issue*, (b) the issue of *finding coherent data patterns*, and (c) the issue of the visual *detection of (non-compact) clusters*.

- (a) *Overplotting Issue*: describes that different data points $\mathbf{d}_i, i = 1, \dots, l$ might map to the same position \mathbf{x} in visualization space by $\bar{\mathbf{x}} = \bar{\mathbf{A}} \cdot \bar{\mathbf{d}}_i$, which causes a loss of information. This effect occurs especially for data being globally or locally dense. Due to the spatial separation, the \mathbf{d}_i are mapped to different positions \mathbf{x}_i when using a projective magic lens if the data records are different, i.e., $\mathbf{d}_i \neq \mathbf{d}_j$. Obviously, the introduced distances $\|\mathbf{x} - \mathbf{x}_i\|$ shrink to 0 if the projective lens strength s vanishes: $s \rightarrow 0 \Leftrightarrow \|\mathbf{x} - \mathbf{x}_i\| \rightarrow 0$. Nevertheless, also multiple overplottings are resolvable iff $s \neq 0$ applies, as Fig. 6(c) suggests.

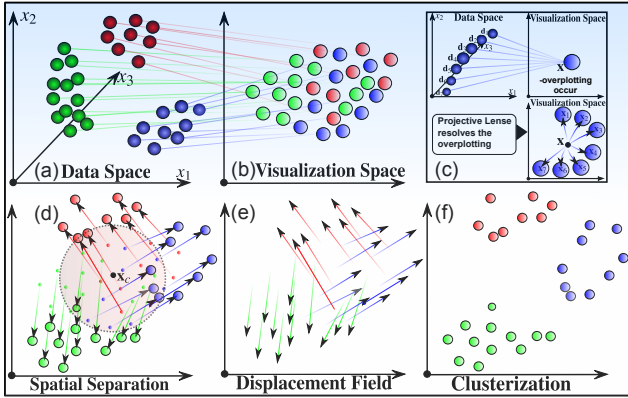


Figure 6: Schematic illustration of the spatial separation by applying our data-driven projective magic lens on a visualization of overlaid data patterns: (a) Considered data with separated colored data cluster. (b) Related projection-based visualization that shows overlaid pattern of the original separated data patterns. (c) Example of an overplotting effect of those data that are separated in data space but mapped to same position in visualization space. Applying the lens resolves the overplotting. (d) Applying of the projective magic lens at position \mathbf{x}_c on the visualization of (b) leads to a spatial separation of the data patterns (cf. (a)) in the visualization space by moving the data representatives along the displacement field of (e). (f) An optimal spatial separation might lead to a visual cluster separation of related patterns of the underlying data.

- (b) Finding Coherent Data Patterns: means that it is desired that separated patterns in the data should also be detectable in visualization and projection space. Usually, this is a challenging task since separated data patterns appear overlaid in visualization space. The spatial separation allows the user to build up a mental image about unrelated data patterns because coherent patterns “move” in a coherent direction during the projective magic lens-based exploration. Hence, a number k of different movement directions – or a discontinuous movement pattern in the underlying displacement field – implies that a number of k separated data patterns is overlaid within the visualizations. This way, unrelated but in the projection overlaid patterns become traceable, as illustrated in Fig. 6(e) for a number of $k = 3$ different displacement patterns.
- (c) Detection of (Non-Compact) Clusters: is one desired aim in visual search, since it, e.g., prepares the analysis of association rules encoded by the data. Regarding this, the spatial separation might lead to a complete separation in visual space of representatives of separated clusters in data space. It enables a cluster analysis w.r.t. a projection configuration of interest that would not be able without the use of our projective magic lens, as illustrated in Fig. 6(f).

We exemplarily illustrate the benefit of projective magic lens concepts compared to traditional magic lens concepts. One family of traditional magic lens concepts are poly-focal magic lenses [KS78, LA94]: Given the center of the lens \mathbf{x}_c , radius r , and strength s , a visual representative \mathbf{x} is replaced to $\mathbf{x}' = \mathbf{x} + \text{mag}(\mathbf{x})_{\mathbf{x}_c, s} \cdot (r \cdot (\mathbf{x} - \mathbf{x}_c) / \|\mathbf{x} - \mathbf{x}_c\|)$ by using a (discrete or continuous) magnification function, e.g., a radial-basis function, such

as $\text{mag}(\mathbf{x})_{\mathbf{x}_c, s} = s \cdot e^{-\|\mathbf{x} - \mathbf{x}_c\|^2}$. See [LA94] for further examples of poly-focal magnification functions. Note that poly-focal magic lenses act in the visualization space only.

In Fig. 7, a comparison between selected results of a real visual exploration with poly-focal and our projective magic lens concept are illustrated for the datasets *Iris*, *Wdbc*, and *Yeast* regarding certain projection configurations. The plain visualizations (Fig. 7 (left)) do not show further structure information. By using our projective magic lens, an underlying clustering of data in visualization space can be revealed, as shown in Fig. 7 (right): For *Iris*, three compact clusters occur, and two rather non-compact clusters occur for *Wdbc*, and *Yeast*. By using the polyfocal magic lens, the underlying clustering stays hidden. In Fig. 8, we provide an additional time series of an interactive visual exploration with both magic lens concepts. The sub-images where clustering occurs are highlighted by green-colored frames. Only magic lenses show further data relations since the data itself is considered for its processing.

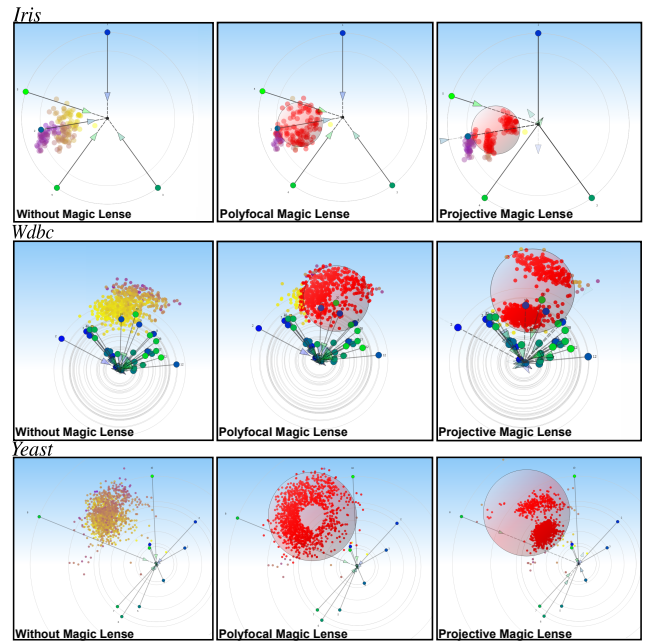


Figure 7: Comparison between different magic lens concepts for a General Projective Map of the *Iris* (top), the *Wdbc* (2nd row), and the *Yeast* (bottom) dataset: (left) without an applied magic lens concept, (middle) with polyfocal magic lens, (right) with our projective magic lens. An inherent clustering in the data appears by using our projective magic lens (right vs. left). With the polyfocal lens the clustering remains hidden (middle vs. right).

5.3. Evaluation of the Distortion Minimization

In this section, we illustrate how our concept of distortion minimization (cf. Sec. 4.2) makes a contribution to an anchor point-based interaction, and we compare it with an interaction that is conducted in projective RadViz, affine Star Coordinates, and Orthographic Star Coordinates [LT13]. Interactively changing anchor points of the projection matrix \mathbf{A} is a frequently used data exploration tool. This is achieved by repositioning an anchor point \mathbf{a}_i and by subsequently updating the projection. Regarding this, in

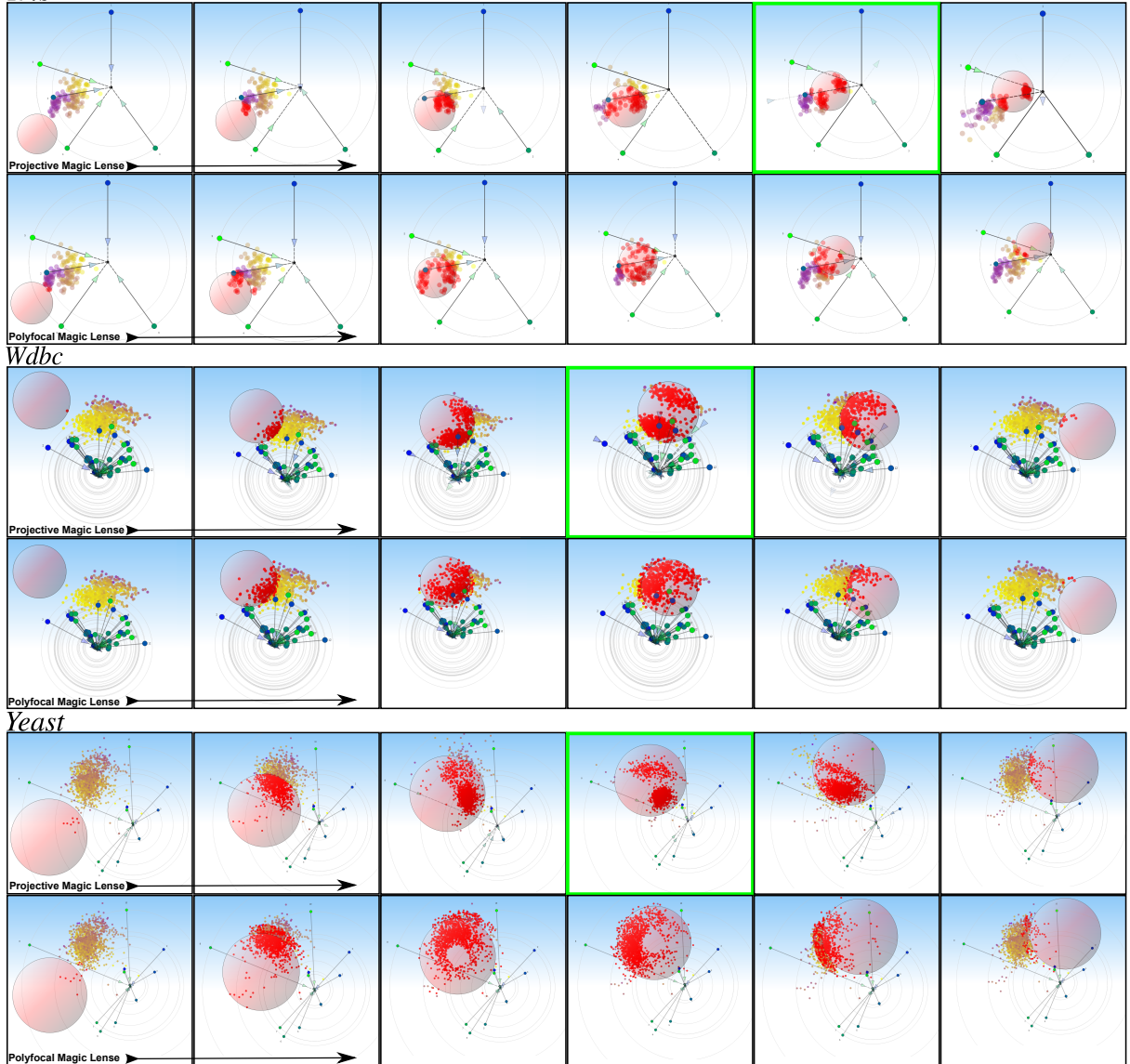
Iris

Figure 8: Time series of our projective (first row per case) and polyfocal (second row per case) magic lenses in action for three cases of the real datasets *Iris* (top), *Wdbc* (middle), *Yeast* (bottom). In contrast to polyfocal lenses, our projective magic lenses allow the visual detection of underlying data patterns, such as, e.g., visually hidden clusters, shown in green-colored frames.

Sec. 5.3.1 we present a systematic analysis for projection properties of both our General Projective Maps in comparison to further projection techniques, and of the choice of distortion minimizing parameters. Following in Sec. 5.3.2, we qualitatively investigate the interaction benefit of General Projective Maps, again in comparison to traditional projection approaches.

5.3.1. Quantitative Evaluation of Distortion Minimization

We empirically evaluate the distortion minimization with the aid of a set of real data application examples. We start with defining a distortion error: Be $\|\mathbf{d}_i - \mathbf{d}_j\| - \|(\mathbf{x}_i/w_i) - (\mathbf{x}_j/w_j)\|$ the pairwise distance differences of pair $(\mathbf{d}_i, \mathbf{d}_j)$ in data space and its related pair $(\mathbf{x}_i/w_i, \mathbf{x}_j/w_j)$ in projection space (cf. Sec 4.2) and be $\text{med}(\cdot)$ the

statistical median value of a set of scalars. Then, with $(\mathbf{x}_i/w_i)^T = (\mathbf{A} \mathbf{c}) \cdot (\mathbf{d}_i^T \mathbf{1})^T$, the average distortion error e_d depending on the projection matrix \mathbf{A} and the projective coefficients \mathbf{c} is given with

$$e_d(\mathbf{A} \mathbf{c}) = |\text{med}(\|\mathbf{d}_i - \mathbf{d}_j\| - \|(\mathbf{x}_i/w_i) - (\mathbf{x}_j/w_j)\|)|.$$

Note that outliers do not negatively influence this median-based measure. Furthermore, outliers are usually not relevant for the visual detection of patterns because data patterns are visually encoded by dense or locally compact regions, which justify the use of the mentioned measure. Thus, if $e_d = 0$ holds, no distortion occurs, except for some outliers, and minimizing e_d would reduce (global) distortion effects.

Experiment 1: We conduct an experiment to evaluate the quality

of distortion minimization regarding our distance minimization in General Projective Maps, and compared to further traditional projection approaches. Our experiment generates a number l of $l = 100$ random projection matrices $\mathbf{A}_i = (a_{ij})$ with $a_{ij} \in [0, \dots, 1]$. Then our experiment defines several projections $\overline{\mathbf{A}}_i^*$ regarding a set of projection concepts for a later analysis on their distortion properties. In detail:

- $\overline{\mathbf{A}}_i^{RV} = (\mathbf{A}_i \mathbf{1})^T$ relates to RadViz,
- $\overline{\mathbf{A}}_i^{SC} = (\mathbf{A}_i \mathbf{0})^T$ relates to Star Coordinates,
- $\overline{\mathbf{A}}_i^{OSC} = (\mathbf{A}_i \mathbf{0})^T$ relates to Orthographic Star Coordinates, with $\mathbf{A}_i = (\mathbf{x}_i \mathbf{y}_i)^T$, $\|\mathbf{x}_i\| = \|\mathbf{y}_i\| = 1$, $\langle \mathbf{x}_i, \mathbf{y}_i \rangle = 0$, where $\langle \mathbf{x}, \mathbf{y} \rangle$ denotes the inner product of vector \mathbf{x} and \mathbf{y} (see [LT13]), and
- $\overline{\mathbf{A}}_i^{GPM} = (\mathbf{A}_i \hat{\mathbf{c}})^T$ related to our General Projective Maps with minimized distortion property, where $\hat{\mathbf{c}}$ are the resulting projective coefficients $\hat{\mathbf{c}}$ that come out when the distortion is minimized, as described by Sec. 4.2.

In order to reveal a statistical view on distortion properties, our experiment calculated the mean average distortion error

$$\bar{e}^* = 1/l \sum_{i=1}^l e_d(\overline{\mathbf{A}}_i^*) \quad (23)$$

and the maximum/minimum distortion error

$$e_{min}^* = \min e_d(\overline{\mathbf{A}}_i^*), e_{max}^* = \max e_d(\overline{\mathbf{A}}_i^*). \quad (24)$$

Our experiments have been conducted with the benchmark data *Iris*, *Wdbc*, and *Yeast*. Fig. 9 illustrates the results.

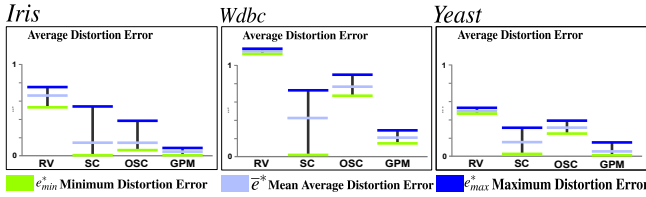


Figure 9: Distortion error values of our Experiments 1 for the datasets *Iris* (top), *Wdbc* (middle), and *Yeast* (bottom) regarding the projection techniques RadViz (RV), Star Coordinates (SC), Orthographic Star Coordinates (OSC), and our distortion minimization of our General Projective Maps (GPM).

Analysis 1: It turns out that the mean average distance error \bar{e}^{GPM} and the maximum error e_{max}^{GPM} for our General Projective Maps is the smallest in any case. These are promising results, meaning that our distance minimization for General Projective Maps generates projections with small distortions. I.e., they are reliable in terms of visual search for patterns, since they are less misleading in a statistical sense within our experiment. The minimum distortion error e_{min}^{GPM} is only in the case of the dataset *Yeast* a bit larger for Star Coordinates than for General Projective Maps. But the difference in between has a dimensionality of 10^{-3} and is negligible.

Interestingly, the mean average distortion error \bar{e}^{OSC} for Orthographic Star Coordinates (OSC) is larger than the related value \bar{e}^{SC} for Star Coordinates in case of the datasets *Wdbc* and *Yeast*. Following [LT13], one would expect the opposite, but an explanation is obvious: OSC guarantees that pairwise distances in data space

do not get larger in projection space, but might be smaller; that would cause a distortion error which explains the observed mean average distortion error behavior. It follows that a large mean average distortion error value does not necessarily have to be a bad result but a small value is always a good result, such as performed by our General Projective Maps. The mean average distortion value \bar{e}^{RV} for RadViz is throughout the largest. RadViz and General Projective Maps are both projective projections but the one performs worse the other quite well regarding distortion reduction, which illustrates that the projective properties need to be steered carefully in order to reduce distortion, which justifies the use of our optimal projective coefficients and our General Projective Maps.

Experiment 2: In addition, we were interested in the question how dependent our distance minimization and the related distortion error is on the choice of the parameters α and β (cf. Sec. 4.2). Hence we conduct another experiment. Analog to Experiment 1, our Experiment 2 generates $l = 100$ random projections $\mathbf{A}_i, i = 1, \dots, l$. For each projection matrix \mathbf{A}_i , a number of optimal distortion minimizing projective coefficients $\hat{\mathbf{c}}_\beta$ were calculated, for the cases $\beta = 0.1, 0.2, \dots, 1.0$ and $\alpha = 0.5$. Since only the ratio of α and β influences the outcome (cf. Sec. 4.2), it is sufficient to fix one parameter and vary the other. We vary β , i.e. the projection $\overline{\mathbf{A}}_{i,\beta}^{GPM} = (\mathbf{A}_i \hat{\mathbf{c}}_\beta)^T$ relates to the General Projective Map which is distortion minimized by the parameter β . The mean average distortion error measure \bar{e}_β^{GPM} and its family $e_{min,\beta}^{GPM}, e_{max,\beta}^{GPM}$ is given analogously to Eq. (23) and Eq. (24). Again, this experiment has been conducted in the data *Iris*, *Wdbc*, and *Yeast*. Fig. 10 illustrates the results.

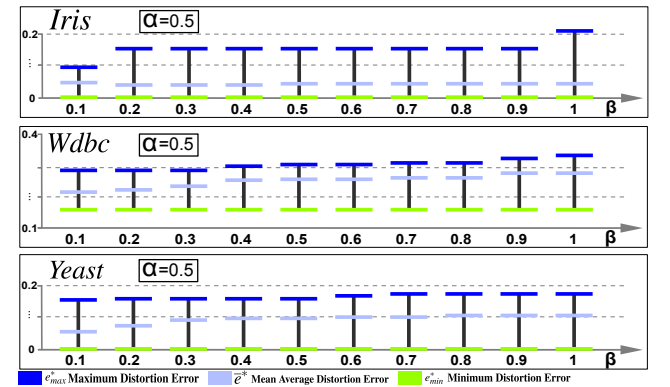


Figure 10: Distortion error values of our Experiment 2 for the dataset *Iris* (top), *Wdbc* (middle), and *Yeast* (bottom) regarding the parameterization α, β of our distortion minimization algorithm for our General Projective Maps. The error value pattern is almost constant and independent of chosen α, β parameters.

Analysis 2: It can be seen that the characteristics \bar{e}_β^{GPM} , $e_{min,\beta}^{GPM}$, and $e_{max,\beta}^{GPM}$ behave quite identical throughout the experiment. In the *Yeast* and *Wdbc* dataset, a slight variation of the mean average distortion error \bar{e}_β^{GPM} can be observed supporting the statement that an appropriate parameter choice for our distortion minimization approach is $\alpha = 0.5$ and $\beta = 0.1$, i.e., a ratio of 5 (0.5/0.1) seems to be reasonable. However, the dependency on these parameters is a weak one. In fact, the algorithm appears to be quite independent of the choice of parameterization.

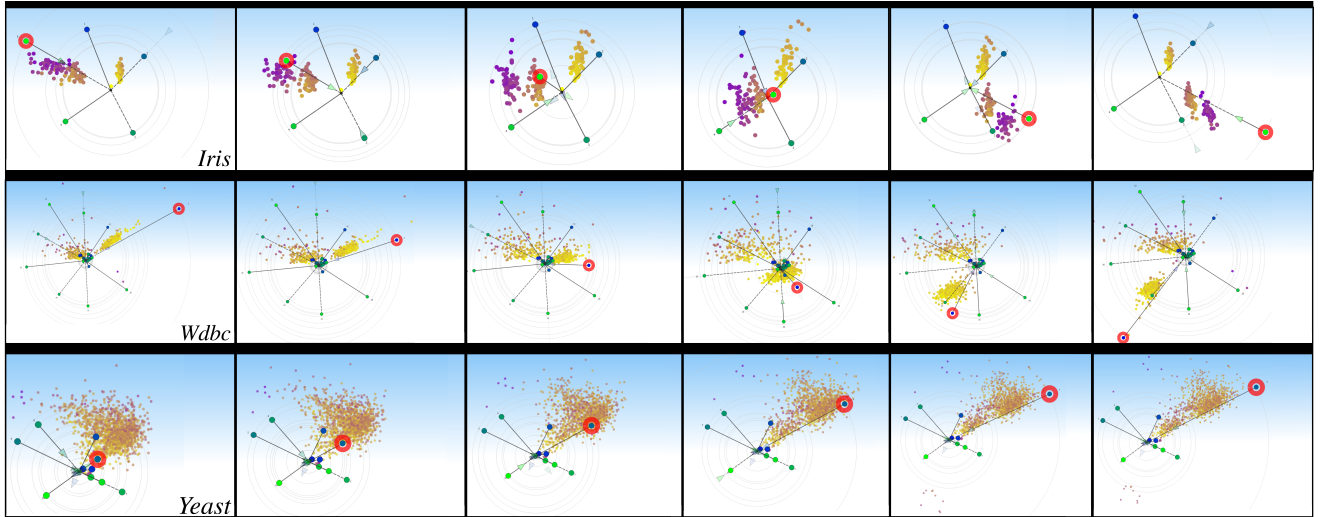


Figure 12: Time series of anchor point interaction (red circle) for our distortion minimization in our General Projective Maps (GPM). We considered the datasets *Iris* (top), *Wdbc* (middle), and *Yeast* (bottom).

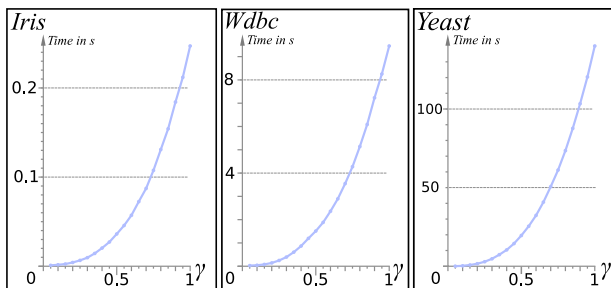


Figure 11: Timings (in second) for the distortion minimization algorithm w.r.t. an increasing data sampling \mathbf{D}_γ with $\gamma = 0.1, \dots, 1$. The performance deteriorates almost quadratically with growing γ .

5.3.2. Qualitative Evaluation of Distortion Minimization

Interaction abilities are important for the practicability of projection approaches [BCL*06, MT03, MFL13, SY06]. To figure out the interaction abilities, we conduct a qualitative experiment by applying anchor point interactions in projection space for our benchmark data. We investigate the interaction of anchor points w.r.t. our General Projective Maps and our distortion minimization approach, which is proceeded in the background. Note that the issue of distortion minimization grows with the number m of data records Eq. (19-21) and might thus be expensive, especially compared to our projective magical lens concept. We follow the suggestion of [PSN10] and we use a uniform data sampling \mathbf{D}_γ of the data \mathbf{D} for Eq. (19-21), whereas $\gamma \in [0, \dots, 1]$ describes the portion of the data \mathbf{D} , i.e., $\mathbf{D}_{0.1}$ equates to 10% of the data, $\mathbf{D}_{0.2}$ equates to 20% of the data, and finally $\gamma = 1$ equates to the complete data $\mathbf{D}_1 = \mathbf{D}$. Fig. 11 illustrates how the performance of our distortion minimization relates to the considered portion γ . Clearly, the algorithm can be used in an interactive mode only if a subset of the data is considered. Thus, we chose \mathbf{D}_γ in a way such that the distortion error for \mathbf{D}_γ and \mathbf{D} behaves similar. In fact, if \mathbf{D}_γ in our studies equates to about 10% ($\mathbf{D}_{0.1}$) of the data values of \mathbf{D} , the distortion error behaves quite equal and the interaction performs well, too (cf. additional

video). Fig. 12 shows a selected set of time series of the anchor point interaction (find further interaction-based time series in the additional material). It turns out that the distortion minimization-based interaction in General Projective Maps introduces two novel characteristic abilities for visual search: (a) *Structure-related Scaling* and (b) *Structure-related Interlinking*.

- (a) *Structure-related Scaling*: Informally speaking, projected points usually “move” within the visualization space during an interaction process regarding traditional projection approaches. In General Projective Maps, a novel interaction-based visual effect occurs: a set of points does an additional scaling under interaction. This is interesting, since data patterns that are separated in data space have different scaling behaviors in projection space under interaction, even if the projected points are overlaid. Thus, separated structures can be revealed by the user. For instance, one set of projected points might “shrink” and another set of points might visually “grow”, which makes the difference of both sets recognizable. Obviously, it is hard to show an effect of movement by single images. Thus, consider the additional video for understanding this scaling effect.
- (b) *Structure-related Interlinking*: Not all projected structures have to have a relation to each data dimension (cf. sub-spaces). Thus, during an interaction some projection points might not be influenced, i.e., “blind” anchors and dimensions, respectively exist (see additional material). Thus, relations between the patterns remain unclear. In the GPM-based interaction all projected patterns are mutually interlinked and thus participate (in each situation) in an interaction, i.e., no “blind” dimensions are possible anymore. This structure-related interlinking facilitates to investigate relations between the patterns, such as relative size in data or compactness abilities, which can be seen in the GPM-based interaction for all benchmark data in Fig. 12.

Note that Orthographic Star Coordinates perform a high-dimensional rotation. Hence, the complete projection configuration is influenced and changed under interaction, i.e., the complete anchor point configuration is continuously transformed. Our Gen-

eral Projective Maps instead allow a visual investigation of global distance-based properties and data patterns with the same and desired projection configuration, i.e., solely the interacting anchor point is transformed, the remaining axes are not influenced.

6. Discussion

Our projection approach integrates the benefits of RadViz and Star Coordinates and facilitates novel data-driven interaction concepts.

Projective Magic Lens: Over-plotting - Standard solutions asked for (i) an appropriate density distribution [MG13] or (ii) an opacity function. This brings up either (i) questions of performance – because data structures have to be maintained and sampling issues occur – or (ii) questions of transfer function design and value normalization [SSK06]. Our concepts avoid these questions by providing a smooth spatial separation of over-plotted data points.

Finding coherent patterns - Standard solutions are based on using a sophisticated distance-based color-coding for the data in the visualization space. Such color-coding is prone to outliers, which might cause a misleading color-coding that falsely points out that no space separated data patterns exist, even though the opposite might be true. Moreover, the visual clutter might be large if many colors are used, and a color-coding is self-defeating for such a case. Our concept avoids such perceptual interferences.

Cluster detection - a hidden clustering might occur under optimal choice of projection configuration only if these clusters in data really exist. In other words, to the best of our knowledge, no false positive detection of clusters is possible.

Distortion Minimizing: Structure-related scaling makes the visual separation of separated data patterns possible, even though the patterns are overlaid in projection space. This enables new data insights and it supports the visual analysis of complex patterns.

Structure-related interlinking enables an action-reaction-like interaction in any case, since distortions in the visualization are continuously minimized.

GPM vs. MDS: A (metric) MDS is looking for one single projection (except rotation and scaling) that minimizes the distortion best (or any other stress function) on a global level. This is equal to a global distortion minimization. From the users' point of view, a MDS yields only one anchor point configuration \mathbf{A}_{MDS} . But what if the user is interested in investigating further anchor point configurations? Thus, it is our idea to allow the user to set up the anchor point configuration in the projection matrix \mathbf{A} , and to use the remaining degree of freedom of $(\mathbf{A}\mathbf{c})^T$ in the \mathbf{c} 's in order to minimize the distortion for this configuration best within our distortion minimization approach. This gives us a local minimum w.r.t. distortion but it allows anchor point interaction. The MDS gives - at least theoretically - a global distortion minimum, but made anchor point interaction impossible by design.

Our magic lens approach allows to select a subset of the data which should be projected as distortion-free as possible regarding a (user-selected) anchor point configuration. It does not optimize the distortion globally, or for all the available data. Quite the contrary, the distortion for the remaining projected data points might increase. Even though the radius r of the lens would be infinite, meaning that all data are considered for distortion minimization, the resulting projection gives again a local minimum w.r.t. the distortion and is thus similar to the result of our interactive distortion minimizing

approach but not to the MDS, since the anchor point configuration is still not part of the optimization itself (but the projective coefficients \mathbf{c}) as it is in the MDS case.

Limitations: Both our magic lens concept and our distortion minimization concept find a local minimum (by fixing \mathbf{A}) for the distortion error function, while the MDS detects a global minimum. Moreover, the interactivity w.r.t. the distortion minimization is enabled as long as a sparse data sampling is used. Using more data samples improves the quality of the distortion minimization but made interaction impossible regarding our hardware configuration setup. Beyond these rather technical limitations, the interpretation of the data is less intuitive for an arbitrary user, since the manner how the projective coefficients behave under interaction can hardly be brought into accordance with the data in a mental sense. Informally speaking, one can visually recognize that something is being optimized but one cannot intuitively understand the relation to the data without more ado.

7. Conclusion

We presented General Projective Maps to unify and extend the traditional (multivariate) projection approaches of projective Radial Visualizations and of affine Star Coordinates. We do so by introducing novel projective coefficients. Additionally, we illustrated that the novel degree of freedom enables both a smooth transition between Radial Visualization and Star Coordinates and a general exploration of the complete space of projective projections. Additionally, we point out and evaluate concepts for an automatic optimization of the projective coefficients, which leads to a concept of an interactive but data-driven projective magic lens and to an interactive global distortion minimization. It enables reliable views to the data pattern and potentially to novel data insights. We tested our approach on a set of high-dimensional benchmark data. There, we were able to detect structures by our techniques which would not have been detected by traditional approaches regarding similar projection configurations.

Acknowledgments: This work was supported and enabled by a grant from the German Research Foundation (LE 3552/1-1).

References

- [ABD*12] AMORIM E., BRAZIL E., DANIELS J., JOIA P., NONATO L., SOUSA M.: iLAMP: Exploring High-Dimensional Spacing through Backward Multidimensional Projection. *IEEE Conf. on Vis. Analytics Sci. Tech. (VAST)* (2012), 53–62. 2
- [AN] ASUNCION A., NEWMAN D.: UCI Machine Learning Repository. 5
- [Asi85] ASIMOV D.: The Grand Tour: a Tool for Viewing Multidimensional Data. *Journal on Scientific and Statistical Computing* 6, 1 (1985), 128–143. 2
- [ATS82] APPERLEY M. D., TZAVARAS I., SPENCE R.: A Bifocal Display Technique For Data Presentation. In *Proc. of Eurographics* (1982), pp. 27–43. 3
- [BCL*06] BORDIGNON A., CASTRO R., LOPES H., LEWINER T., TAVARES G.: Exploratory Visualization based on Multidimensional Transfer Functions and Star Coordinates. In *XIX Brazilian Symposium on Computer Graphics and Image Processing* (2006), pp. 273 – 280. 9
- [CBCH95] COOK D., BUJA A., CABRETA J., HURLEY C.: Grand tour and projection pursuit. *Journal of Computational and Statistical Computing* 4, 3 (1995), 155–172. 2
- [CCKT83] CHAMBERS J., CLEVELAND W. S., KLEINER B., TUKEY P. A.: *Graphical Methods for Data Analysis*. Chapman & Hall, 1983. 1

- [CM15] CHENG S., MUELLER K.: Improving the Fidelity of Contextual Data Layouts using a Generalized Barycentric Coordinates Framework. In *IEEE Pacific Visualization* (2015), pp. 295–302. 2
- [CM16] CHENG S., MUELLER K.: The Data Context Map: Fusing Data and Attributes into a Unified Display. *IEEE Trans. Vis. Comput. Graph.* 22, 1 (2016), 121–130. 2
- [DCFMFM10] DI CARO L., FRIAS-MARTINEZ V., FRIAS-MARTINEZ E.: Analyzing the Role of Dimension Arrangement for Data Visualization in RadViz. In *Proc. of the 14th Pacific-Asia conference on Advances in Knowledge Discovery and Data Mining - Volume Part II* (2010), pp. 125–132. 1, 2
- [DGRG12] DANIELS K. M., GRINSTEIN G. G., RUSSELL A., GLIDEN M.: Properties of Normalized Radial Visualizations. *Information Visualization* 11, 4 (2012), 273–300. 1, 2
- [EHM*11] ENDERT A., HAN C., MAITI D., HOUSE L., LEMAN S., NORTH C.: Observation-level Interaction with Statistical Models for Visual Analytics. In *IEEE Conf. on Vis. Analytics Sci. and Tech. (VAST)* (2011), pp. 121–130. 2
- [EMdSP*15] ETEMADPOUR R., MOTTA R., DE SOUZA PAIVA J. G., MINGHIM R., DE OLIVEIRA M. C. F., LINSEN L.: Perception-based Evaluation of Projection Methods for Multidimensional Data Visualization. *Proc. IEEE Information Visualization* (2015). 2
- [Far02] FARIN G.: *Curves and Surfaces for CAD: A Practical Guide*, 5th ed. Morgan Kaufmann Publishers Inc., 2002. 1, 2, 3
- [FB95] FURNAS G. W., BEDERSON B. B.: Space-Scale Diagrams: Understanding Multiscale Interfaces. In *Proc. of CHI-95* (1995), pp. 234–241. 3
- [Fis36] FISHER R. A.: The Use of Multiple Measurements in Taxonomic Problems. *Annals of Eugenics* (1936). 5
- [Fri87] FRIEDMAN J. H.: Exploratory Projection Pursuit. *Journal of the American Statistical Association* 82, 397 (1987), 249–266. 2
- [Fri91] FRIENDLY M.: *SAS System for Statistical Graphics*, 1st ed. SAS Publishing, 1991. 1
- [FT74] FRIEDMAN J. H., TUKEY J. W.: A Projection Pursuit Algorithm for Exploratory Data Analysis. *IEEE Trans. Comput.* 23 (1974), 881–890. 2
- [Fur86] FURNAS G. W.: Generalized Fisheye Views. In *Human Factors in Computing Systems CHI'86 Conference Proc.* (1986), pp. 16–23. 3
- [HGM*97] HOFFMAN P., GRINSTEIN G., MARX K., GROSSE I., STANLEY E.: DNA Visual and Analytic Data Mining. In *Proc. of the 8th conference on Visualization* (1997), pp. 437–ff. 1
- [HGP99] HOFFMAN P., GRINSTEIN G., PINKNEY D.: Dimensional Anchors: a Graphic Primitive for Multidimensional Multivariate Information Visualizations. In *Workshop on New Paradigms in Information Visualization and Manipulation* (1999), pp. 9–16. 1
- [IMI*10] INGRAM S., MUNZNER T., IRVINE V., TORY M., BERGNER S., MÖLLER T.: DimStiller: Workflows for Dimensional Analysis and Reduction. *IEEE Conf. Vis. Analytics Sci. Tech.* (2010), 3–10. 1
- [IMO09] INGRAM S., MUNZNER T., OLANO M.: Glimmer: Multilevel MDS on the GPU. *IEEE Trans. Vis. Comput. Graph.* (2009), 249–ff. 2
- [JCC*11] JOIA P., COIMBRA D., CUMINATO J. A., PAULOVICH F. V., NONATO L. G.: Local Affine Multidimensional Projection. *IEEE Trans. Vis. Comput. Graph.* 17, 12 (2011), 2563–2571. 2
- [JZF*09] JEONG D. H., ZIEMKIEWICZ C., FISHER B. D., RIBARSKY W., CHANG R.: iPCA: An Interactive System for PCA-based Visual Analytics. *Comput. Graph. Forum* 28, 3 (2009), 767–774. 2
- [Kan00] KANDOGAN E.: Star Coordinates: A Multi-Dimensional Visualization Technique with Uniform Treatment of Dimensions. *IEEE Information Visualization* (2000), 9–12. 1, 2
- [Kan01] KANDOGAN E.: Visualizing Multi-Dimensional Clusters, Trends, and Outliers Using Star Coordinates. In *Proc. of the seventh ACM SIGKDD international Conference on Knowledge Discovery and Data Mining* (2001), 107–116. 2
- [KS78] KADMON N., SHLOMI E.: A Polyfocal Projection for Statistical Surfaces. *The Cartographic Journal* 15, 1 (1978), 36–41. 6
- [LA94] LEUNG Y. K., APPERLEY M. D.: A Review and Taxonomy of Distortion-oriented Presentation Techniques. *ACM Trans. Comput.-Hum. Interact.* 1, 2 (1994), 126–160. 5, 6
- [LT13] LEHMANN D. J., THEISEL H.: Orthographic Star Coordinates. *IEEE Information Visualization* 19, 12 (2013), 2615–2624. 1, 2, 6, 8
- [LT15] LEHMANN D. J., THEISEL H.: Optimal Sets of Projections of High-Dimensional Data. *IEEE Information Visualization* (2015). 2
- [MFL13] MOLCHANOV V., FOFONOV A., LINSEN L.: Continuous Representation of Projected Attribute Spaces of Multifields over Any Spatial Sampling. In *Proc. Eurovis* (2013), vol. 32, pp. 301–310. 9
- [MG13] MAYORGA A., GLEICHER M.: Splatterplots: Overcoming Overdraw in Scatter Plots. *IEEE Trans. Vis. Comput. Graph.* 19, 9 (2013), 1526–1538. 10
- [MT03] MA K.-L., TEOH S. T.: StarClass: Interactive Visual Classification Using Star Coordinates. In *Proc. of the 3rd SIAM International Conference on Data Mining* (2003), pp. 178–185. 9
- [NK91] NAKAI K., KANEHISA M.: Expert System for Predicting Protein Localization Sites in Gram-Negative Bacteria. *Proteins: Structure, Function and Genetics* 11, 2 (1991), 95–110. 5
- [NM13] NAM J., MUELLER K.: A Tourism-Inspired High-Dimensional Space Exploration Framework with Overview and Detail. *IEEE Trans. Vis. Comput. Graph.* 19 (2013), 291–305. 2
- [Nov09] NOVÁKOVÁ L.: *Visualization Data for Data Mining*. PhD thesis, Czech Technical University in Prague Faculty of Electrical Engineering, Department of Cybernetics, Prague, Czech, 2009. 2
- [Nov06] NOVÁKOVÁ L., ŠTĚPÁNKOVÁ O.: Multidimensional Clusters in RadViz. In *Proc. of the 6th WSEAS International Conference on Simulation, Modelling and Optimization* (2006), World Scientific and Engineering Academy and Society (WSEAS), pp. 470–475. 1, 2
- [Nov11] NOVÁKOVÁ L., ŠTĚPÁNKOVÁ O.: Visualization of Trends Using RadViz. *Journal of Intelligent Information Systems* 37, 3 (2011), 355–369. 2
- [PSN10] PAULOVICH F. V., SILVA C. T., NONATO L. G.: Two-Phase Mapping for Projecting Massive Data Sets. *IEEE Trans. Vis. Comput. Graph.* 16, 6 (2010), 1281–1290. 2, 9
- [RSDRS15] RUBIO-SANCHEZ M., DIAZ F., RAYA L., SANCHEZ A.: A Comparative Study between RadViz and Star Coordinates. *IEEE Trans. Vis. Comput. Graph.* (2015). 2
- [SDMT15] STAHNKE J., DOERK M., MULLER B., THOM A.: Probing Projections: Interaction Techniques for Interpreting Arrangements and Errors of Dimensionality Reductions. *IEEE Information Visualization* (2015). 2
- [SSK06] SCHNEIDEWIND J., SIPS M., KEIM D.: Pixnostics: Towards Measuring the Value of Visualization. *Symp. Vis. Analytics Sci. Tech.* (2006), 199–206. 10
- [SWM93] STREET W., WOLBERG W., MANGASARIAN O.: Nuclear Feature Extraction for Breast Tumor Diagnosis. *SPIE International Symposium on Electronic Imaging: Science and Technology* (1993), 861–870. 5
- [SY06] SHAIK J., YEASIN M.: Visualization of High Dimensional Data Using an Automated 3D Star Coordinate System. *IEEE International Joint Conference on Neural Networks* (2006), 2318–2325. 9
- [TC90] TYLER C., CLARKE M.: The Autostereogram. *Stereoscopic Displays and Applications 1258* (1990), 182–196. 5
- [TGK*14] TOMINSKI C., GLADISCH S., KISTER U., DACHSELT R., SCHUMANN H.: A Survey on Interactive Lenses in Visualization. In *EuroVis State-of-the-Art Reports* (2014). 3
- [TK98] THEISEL H., KREUSELER M.: An Enhanced Spring Model for Information Visualization. *Proc. Eurographics* 17, 3 (1998), 335–344. 2
- [Tor52] TORGERSON W. S.: Multidimensional scaling: I. Theory and Method. *Psychometrika* 17 (1952), 401–419. 2